Paladini, A., & Weber, G. (1981) *Biochemistry 20*, 2587–2593.
Polisky, B. (1989) *Cell 55*, 929–932.
Stavrianopolis, J. G., & Chargaff, E. (1973) *Proc. Natl. Acad. Sci. U.S.A. 70*, 1959–1963.
Stavrianopolis, J. G., & Chargaff, E. (1978) *Proc. Natl. Acad. Sci. U.S.A. 75*, 4140–4144.
Stein, H., & Hausen, P. (1969) *Science 165*, 393–395.
Stephano, J. L., Gould, M., & Rojas-Galicia, L. (1986) *Anal. Biochem. 152*, 308–313.
Wada, K., Sawai, Y., & Tsukada, K. (1980) *Biochim. Biophys. Acta 612*, 253–261.
Wyers, F., Sentenac, A., & Fromageot, P. (1973) *Eur. J. Biochem. 35*, 270–281.
Wyers, F., Huet, J., Sentenac, A., & Fromageot, P. (1976) *Eur. J. Biochem. 69*, 385–395.

Crystal Structures of Phosphonoacetamide Ligated T and Phosphonoacetamide and Malonate Ligated R States of Aspartate Carbamoyltransferase at 2.8-Å Resolution and Neutral pH[†,‡]

J. Eric Gouaux and William N. Lipscomb*
Gibbs Chemical Laboratory, Harvard University, Cambridge, Massachusetts 02138
Received June 19, 1989; Revised Manuscript Received August 29, 1989

ABSTRACT: The T → R transition of the cooperative enzyme aspartate carbamoyltransferase occurs at pH 7 in single crystals without visibly cracking many of the crystals and leaving those uncracked suitable for single-crystal X-ray analysis. To promote the T → R transition, we employ the competitive inhibitors of carbamoyl phosphate and aspartate, which are phosphonoacetamide (PAM) and malonate, respectively. In response to PAM binding to the T-state crystals, residues Thr 53–Thr 55 and Pro 266–Pro 268 move to their R-state positions to bind to the phosphonate and amino group of PAM. These changes induce a conformation that can bind tightly the aspartate analogue malonate, which thereby effects the allosteric transition. We prove this by showing that PAM-ligated T-state crystals (T_{pam}), space group *P*321 (a = 122.2 Å, c = 142.2 Å), when transferred to a solution containing 20 mM PAM and 8 mM malonate at pH 7, isomerize to R-state crystals ($R_{pam,mal,soak}$), space group also *P*321 (a = 122.2 Å, c = 156.4 Å). The R-state structure in which the T → R transition occurs within the crystal at pH 7 compares very well (rms = 0.19 Å for all atoms) with an R-state structure determined at pH 7 in which the crystals were initially grown in a solution of PAM and malonate at pH 5.9 and subsequently transferred to a buffer containing the ligands at pH 7 ($R_{pam,mal,crys}$). In fact, both of the PAM and malonate ligated R-state structures are very similar to both the carbamoyl phosphate and succinate or the *N*-(phosphonoacetyl)-L-aspartate ligated structures, even though the R-state structures reported here were determined at pH 7. Crystallographic residuals refined to 0.16–0.18 at 2.8-Å resolution for the three structures.

Aspartate carbamoyltransferase [from *Escherichia coli*, EC 2.1.3.2; for a recent review, see Kantrowitz and Lipscomb (1988)] catalyzes the formation of phosphate and *N*-carbamoyl-L-aspartate from carbamoyl phosphate and L-aspartate, initiating the first step in the synthesis of pyrimidines (Jones et al., 1955; Reichard & Hanshoff, 1956). In response to saturating concentrations of substrates, the enzyme undergoes large conformational rearrangements in the T → R[1] transition as illustrated and described in Figure 1. The changes in the quaternary structure of the molecule as a result of the allosteric transition are evident in the difference of the c axis unit cell dimensions of *P*321 crystals. For the T state the c axis length is 142 Å, and for the R state the length is 156 Å; the length of the a axis of 122 Å changes less than 0.5 Å as a result of the transition. The increase in the c-axis dimension of the R-state crystals, consistent with a molecular expansion along c by 8 Å, was noted by Monaco (Monaco, 1978; Monaco et al., 1978). Ultracentrifugation experiments that demonstrated an increase in the frictional coefficient of the enzyme in the presence of *N*-(phosphonoacetyl)-L-aspartate (PALA) were interpreted in terms of a 3.5% expansion of a spherical model or an expansion (or contraction) of an ellipsoid model (Gerhart & Schachman, 1968). Moody et al. (1979) predicted the

[†] This work was supported by the National Institutes of Health (Grant GM06920).

[‡] The coordinates of all structures have been submitted to the Brookhaven Protein Data Bank. The entry names for the coordinates are as follows: 1AT1 ATC (PAM and malonate ligated R state, crystal soak); 2AT1 ATC (PAM and malonate ligated R state, cocrystal); 3AT1 ATC (PAM ligated T state).

[1] T is an abbreviation for tense and is used here to indicate the conformational state of the enzyme that has unit cell dimensions of a = 122 Å and c = 142 Å in the space group *P*321; R, an abbreviation for relaxed, indicates the conformational state of the enzyme that has unit cell dimensions of a = 122 Å and c = 156 Å also in the space group *P*321. To signify that a structure contains a ligand bound at the active site, we will add an abbreviation of the ligand name as a subscript to either T or R. Alternatively, if the ligand is bound to the regulatory site, then an abbreviation for that ligand will be added as a superscript. Functionally, the T form shows low activity and low aspartate affinity, while the R form has a high activity and a high affinity for aspartate. See Monod et al. (1965) for a discussion on a theory of allosteric transitions in proteins and for an explanation of the nomenclature.

0006-2960/90/0429-389$02.50/0

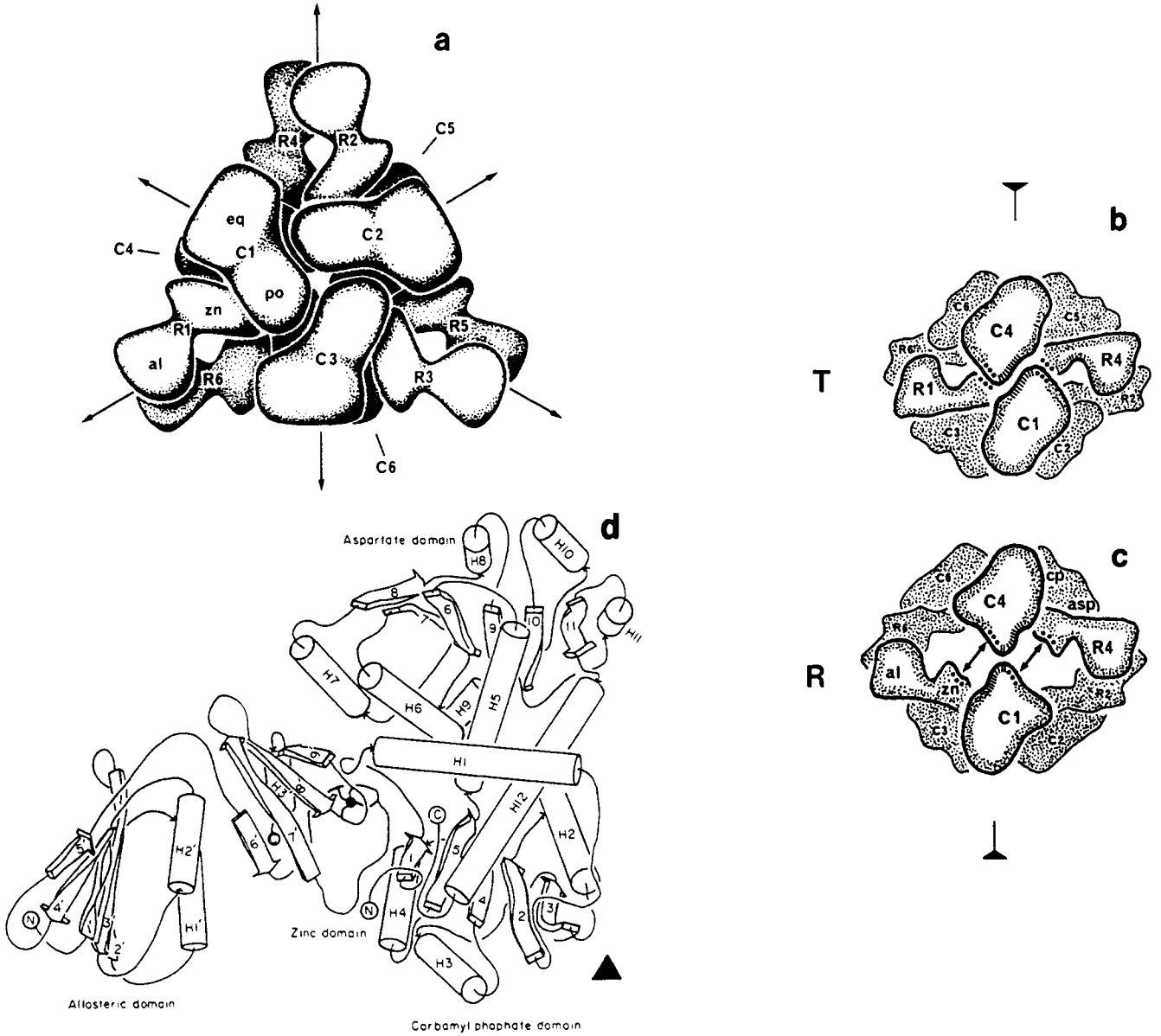

FIGURE 1: (a) Comprising the dodecameric enzyme are two catalytic trimers, each composed of three catalytic chains (C1, C2, C3; C4, C5, C6), and three regulatory dimers, each made up of two regulatory chains (R1, R6; R2, R4; R3, R5); the five oligomers are arranged with approximate D_3 symmetry in the *P*321 crystal forms discussed in this paper (Wiley & Lipscomb, 1968). Contained in the asymmetric unit of the *P*321 space group are two catalytic chains, one residing in the upper catalytic trimer and the other in the lower catalytic trimer, and two regulatory chains, comprising one regulatory dimer; the crystallographic 3-fold operation then produces the complete upper and lower catalytic trimers and the two other regulatory dimers. The locations of the carbamoyl phosphate (cp), aspartate (asp), zinc (zn) and allosteric domains are also indicated. Here, the molecule is oriented such that the 3-fold axis is perpendicular to the plane of the page. (b), (c) T and R quaternary structures arranged with the 3-fold axis in the plane of the page and one of the 2-fold axes perpendicular to the plane of the page. As a result of the T → R transition, the separation between the catalytic trimers increases by 12 Å along the 3-fold axis while the trimers rotate 5° in opposite directions around the same axis; each of the three regulatory dimers rotates by 15° about the three 2-fold axes. The asterisks indicate the surface of the enzyme involved in the C1–R4 and C4–R1 interfaces, and the slashes define the regions involved in the C1–C4 contacts. We draw your attention to the differences in these interfaces in the T and R states. (d) Secondary structural elements of one catalytic and one regulatory chain of aspartate carbamoyltransferase. The location of the 3-fold axis is indicated by the black triangle, and its orientation is perpendicular to the page. The definitions of the helices and β-strands were derived from Kim et al. (1987). The active site is located between the carbamoyl phosphate and the aspartate domains.

10–12-Å expansion from an analysis of PALA-induced structural changes, using the known structure of the T state of the enzyme and low-angle X-ray scattering data; however, the rotations of the subunits and domains were not correctly anticipated.

The kinetic mechanism of the holoenzyme at pH 7.0 can be described as "preferred order", where carbamoyl phosphate binds first, aspartate binds next, *N*-carbamoyl-L-aspartate is released first, and phosphate is released last (Porter et al., 1969; Wedler & Gasser, 1974; Jacobson & Stark, 1975; Hsuanyu & Wedler, 1987). Evidence for changes in the properties of the catalytic trimer or the holoenzyme upon ligation by carbamoyl phosphate comes from ultraviolet difference spectroscopy (Collins & Stark, 1969), circular dichroism (Griffin et al., 1972, 1973), dissociation induced by sodium dodecyl sulfate (Colman & Markus, 1972), and chemical modification experiments (Gerhart & Schachman, 1968). Indeed, ligation of the holoenzyme with carbamoyl phosphate increases the stability of the R state relative to that of the T state by 2.1 kcal/mol (Howlett et al., 1977).

Ligation of the enzyme with phosphonoacetamide (PAM, K_i = 0.66 mM at pH 8 for the catalytic trimer; Porter et al.,

1969), a competitive inhibitor of carbamoyl phosphate, produces small conformational changes that do not trigger the T → R rearrangement but are nonetheless required for the subsequent tight binding of malonate, a competitive inhibitor of aspartate, which then induces the T → R transition. Crystallization and crystal-soaking experiments have shown that malonate will induce the T → R transition only if phosphonoacetamide (PAM) or carbamoyl phosphate is also present. We identify the conformational changes that PAM induces by determining the structure of its complex with the enzyme (T_{pam}) at 2.8-Å resolution by X-ray crystallography. We also prove that the conformation of the PAM-ligated enzyme in the crystal is cooperatively competent by binding malonate to the T_{pam} crystal and inducing the allosteric transition at pH 7. Finally, we compare the structure of the R-state enzyme ligated with PAM and malonate, where the T → R transition occurred within the crystal ($R_{pam,mal,soak}$), to another R-state enzyme ($R_{pam,mal,crys}$) whose structure was determined from crystals grown in the presence of PAM and malonate at pH 5.8 which were later transferred to a PAM and malonate buffer at pH 7.

Experimental Procedures

Materials. 4-Morpholineethanesulfonic acid (MES), ethylenediaminetetraacetic acid (EDTA), sodium azide, 2-mercaptoethanol, polyethyleneglycol 8000 (PEG 8000), succinic acid, aspartic acid, and malonate were purchased from Sigma Chemical Co. and were used without further purification. Diethylphosphonoacetamide was purchased from K & K Laboratories, Division of ICN Biomedicals, Inc. Tetrahydrofuran, CaH_2, bromotrimethylsilane, phosphorous pentoxide, methanol, and acetone were purchased from Aldrich Chemical Co. Native aspartate carbamoyltransferase was isolated as described (Nowlan & Kantrowitz, 1985) from the EK1104 strain of *E. coli* which contained the plasmid pEK2 carrying the entire native *pyrBI* operon, in the laboratory of E. R. Kantrowitz.

Phosphonoacetamide Synthesis. To a flame-dried 50-mL round-bottom flask under positive N_2 atmosphere was added 10 mL of tetrahydrofuran (distilled from CaH_2) and 1.95 g of diethylphosphonoacetamide (10 mmol; dried for 24 h, in vacuo, in the presence of phosphorous pentoxide). The flask was cooled to 0 °C in an ice/water bath, and subsequently 3.1 g (20 mmol) of freshly distilled bromotrimethylsilane was added to the reaction flask via a syringe. After reaction at 0 °C for 1 h, the ice/water bath was removed, and the reaction was allowed to continue for an additional 2 h at room temperature. During this time the reaction mixture turned from a colorless, clear solution to a pale yellow, clear solution. The solution was then concentrated, and 25 mL of dry acetone was added to the viscous oil. Hydrolysis of the disilyl phosphonate was effected by the addition of 0.72 g (40 mmol) of distilled water. Immediately following this addition, the white crystalline product precipitated from solution. Purification of the free acid of phosphonoacetamide (PAM) consisted of evaporation of the solvent and recrystallization of the white precipitate from a mixture of methanol and acetone. Following purification, 1.08 g of material was obtained, giving a 75% yield. The molecular structure of PAM was confirmed by ^1H NMR, infrared spectroscopy, and elemental analysis. The melting point of 168 °C compared well with that of 171 °C found previously by Balsiger et al. (1959). This "one pot" synthesis of PAM provided a substantially more efficacious route to the product than did previous syntheses.

Crystal Preparation. The T_{pam} form was prepared by growing T-state crystals at pH 5.8 (Gouaux & Lipscomb, 1989a), transferring the crystals to the presoak buffer [40 mM MES, 3 mM sodium azide, 2 mM 2-mercaptoethanol, and 15% (w/v) polyethylene glycol 8000, pH 7.0, with NaOH] for a minimum of 24 h to dilute the concentration of citrate present in the crystallization buffer. The crystals were then placed in a buffer containing 20 mM PAM, 10 mM MES, 3 mM sodium azide, 2 mM 2-mercaptoethanol, and 15% (w/v) PEG 8000 with the pH adjusted to 7.0 with NaOH; they were soaked in this buffer for 9 days. The $R_{pam,mal,soak}$ crystals were prepared in an identical fashion except that 2 days prior to data collection the crystals were transferred to the transition buffer (20 mM PAM, 8 mM malonate, 10 mM MES, 3 mM sodium azide, 2 mM 2-mercaptoethanol, and 15% PEG 8000 at pH 7.0). These conditions induced the T → R transition. Interestingly, some of these crystals developed circular cracks just inside the perimeter of the hexagonal plate as a result of being placed in the PAM and malonate buffer. However, the cracked region could be removed, as described below. The $R_{pam,mal,crys}$ crystals were prepared by crystallizing the enzyme at a concentration of 15 mg/mL in a buffer containing 20 mM PAM, 20 mM malonate, and 3 mM sodium azide, the pH of which was adjusted to 5.8 with *N*-ethylmorpholine. Hexagonal bars of dimension 0.7 × 0.7 × 1.5 mm grew in 1–2 weeks. After growth, these R-form crystals were then transferred to a buffer that was identical with the transition buffer described above.

Crystallization trials involving other substrate and inhibitor combinations, such as PAM and aspartate, PAM and succinate, and PAM and malic acid, were performed at both pH 5.8–6.0 and pH 7.0–7.8. For the crystallizations carried out at lower pH no precipitating agent was employed. However, PEG 8000 was used in the crystallizations carried out at pH 7.0–7.8.

Data Collection, Scaling, and Reduction. The X-ray diffraction data from these three derivatives were collected at the Biotechnology Resource, University of Virginia, on the multiwire area X-ray diffractometer (Sobottka et al., 1984) as previously described (Gouaux & Lipscomb, 1989b). The integrated intensities from each data set were corrected for background, polarization, and Lorentz factors and then scaled by using the method of Fox and Holmes (1968) as implemented in the CCP4 program package. Table I summarizes the data collection statistics. Due to crystal size, crystal quality, and time constraints at the data collection facility, X-ray diffraction data for these derivatives were measured to 2.8-Å resolution. The data at higher resolution had an unacceptably low signal to noise ratio.

Structure Refinement. All three structures were solved by using the molecular replacement method. The initial model for the T_{pam} structure was derived from the refinement of the CTP ligated T structure (T^{ctp}) against 35000 reflections between 10.0 and 2.5 Å resolution by using the computer refinement program XPLOR (Brünger et al., 1987; Brünger, 1988). The model for the T^{ctp} structure was obtained from the exhaustively refined structure of Kim et al. (1987). We re-refined that structure using XPLOR for a number of reasons. First, we collected a higher resolution, a stronger, and a more complete data set from the CTP-ligated crystals at the Biotechnology Resource at the University of Virginia (Gouaux and Lipscomb, unpublished results). Second, XPLOR does a better job of restraining the van der Waals contacts between atoms than does the refinement programs that Kim et al. (1987) employed. And finally, we wanted to compare the results of the XPLOR refined structure to the structure refined by Kim et al. (1987) to judge whether the two refinements

Table I

form[a]	unit cell	resolution (Å)	measurements[b]	reflections[c]	R^d
T_{pam}	a = 122.4 Å c = 142.2 Å	2.8–6.0	73039	22745 (87%)	0.079
$R_{pam,mal,soak}$	a = 122.3 Å c = 156.4 Å	2.8–6.0	49208	20758 (72%)	0.086
$R_{pam,mal,crys}$	a = 122.2 Å c = 156.6 Å	2.8–6.0	58554	22862 (79%)	0.067

[a] T_{pam}, phosphonoacetamide (PAM) ligated T form of aspartate carbamoyltransferase at pH 7.0; $R_{pam,mal,soak}$, PAM and malonate ligated R form of the enzyme where the T → R transition took place within the crystal at pH 7.0; $R_{pam,mal,crys}$, PAM and malonate ligated R-form structure where the crystals were grown at pH 5.8 in the presence of the ligands and then the crystals were transferred to a buffer at pH 7.0 and the X-ray diffraction data collected, as described in the text. [b] Listed are the total number of observations. [c] Shown are the number of unique reflections and given in parentheses are the ratios of the number of observed reflections to the theoretical number of reflections possible, multiplied by 100. [d] $R_{merge} = \sum_{hkl}(\sum_i|I - \bar{I}|/\sum_i I)$.

yielded different structures. In fact, we discovered no significant differences between the two structures (Gouaux, Kosman, and Lipscomb, unpublished results). The refined carbamoyl phosphate and succinate structure ($R_{cp,suc}$; Gouaux & Lipscomb, 1988), with carbamoyl phosphate and succinate and all of the waters deleted from the coordinate list, was the starting structure for the $R_{pam,mal,soak}$ refinements. The $R_{pam,mal,soak}$ model was then used at the beginning of the $R_{pam,mal,crys}$ refinement.

All refinements were carried out by using the computer program XPLOR running on either a CRAY XMP or a CRAY YMP at the Pittsburgh Supercomputer Center. The stereochemical restraints imposed on the structures consisted of the default bond, angle, torsion, improper, and van der Waals energy functions as defined in version 1.5 of XPLOR. The bond lengths and angles for the zinc–sulfur interactions in the regulatory chain were derived from a small-molecule crystal structure (Swenson et al., 1978). These values for the zinc–sulfur bond lengths are in agreement with the average values as determined from EXAFS experiments on aspartate carbamoyltransferase (Phillips et al., 1982). We empirically adjusted the force constants on the bond and angle terms for the zinc–sulfur cluster to maintain an approximate tetrahedral geometry. The model for the dianionic form of malonate was derived from the crystal structure of a malonate and cobalt complex (Butler & Snow, 1976). The mean values for the C–O bond lengths were determined by applying the Speakman rule (Manojlovic & Speakman, 1967), which states that the sum of the C–O distances for a carboxylic acid will be 2.52 ± 0.02 Å. The bond length and bond angle parameters for PAM were derived from the crystal structure of PALA (Zanotti et al., 1984). The other parameters for the ligands' potential energy functions were obtained from INDO molecular orbital calculations. However, to preclude biasing the model by including the Coulombic energy functions, we turned off the charges on the ligand atoms.

The first round of refinement consisted of the preparation stage, heating stage, cooling stage, and final stage (Brünger 1988), throughout which the electrostatic terms for the side-chain groups for the residues Asp, Glu, Arg, and Lys were turned on. However, we became concerned that the charges on those residues might result in interactions if not inconsistent with, at a minimum not completely defined by, the X-ray data. To ensure that salt links and hydrogen bonds were not "forced" upon the model by the charges on the Asp, Glu, Arg, and Lys residues, we subjected the models to an additional 80 cycles of Powell minimization with the charges on the side chains of these residues turned off. During the refinements of the structures described here, we did not refine the atomic temperature factors. At this stage, $F_o - F_c$ and $2F_o - F_c$ maps were calculated, allowing the ligands and a few solvent molecules in the active site to be built into the map; the fit of the protein atoms to the electron density was also checked at this time.

Table II

form[a]	total atoms	reflections[b]	R_{factor}[c]	rms_{bond}[d] (Å)	rms_{angle}[d] (deg)
T_{pam}	7128	19708	0.181	0.019	3.70
$R_{pam,mal,soak}$	7130	16203	0.164	0.017	3.50
$R_{pam,mal,crys}$	7130	20174	0.170	0.016	3.37

[a] As defined in Table I. [b] The number of reflections used in the refinements with $I \geq 2\sigma(I)$. [c] $R_{factor} = \sum_{hkl}(||F_o| - |F_c||/|F_o|)$. [d] The rms deviations of bond lengths and three atom bond angles from the default parameters contained in version 1.5 of XPLOR.

Table III

ligands	concn (mM)	pH	space group	state
PAM	20	5.8	*P*321	T
PAM	20	7.0	*R*32	T
PAM/aspartate	20/80	5.8	*P*321	T
PAM/aspartate	20/80	7.0	*R*32	T
PAM/succinate	20/60	5.8	*P*321	T
PAM/succinate	20/60	7.0	*R*32	T
PAM/malonate	20/5	5.8	*P*321	R
PAM/malonate	20/40	5.8	*P*321	R

To fit the ligands, solvent, and protein atoms to the electron density, we used the computer graphics program FRODO (Jones, 1982) in a somewhat modified form (Pflugrath et al., 1984), running on an Evans and Sutherland PS300 interfaced to a VAX 11/780. The computer program SUPERIMP (Honzatko, 1986) or XPLOR (Brünger, 1988; Kabsch, 1976) was employed to superimpose and perform the subsequent analysis of all of the structures described here.

Results

Crystallization and Crystal-Soaking Experiments. As documented in Table III, many crystallization and crystal-soaking experiments were performed to determine combinations of substrates and substrate analogues that would induce the T → R transition. Because carbamoyl phosphate readily decomposes in solution (its half-life is about 10 h; Gouaux & Lipscomb, 1988), we decided to use phosphonoacetamide (PAM), which is a stable analogue of carbamoyl phosphate. Crystallizations in the presence of PAM at pH 5.8 or pH 7.0 generally yielded either an octahedral-habit crystal that diffracted only to 7.0 Å or an *R*32 crystal that diffracted to about 3.0 Å. On rare occasions, a poorly formed *P*321 hexagonal plate crystal would grow. These crystals were isomorphous to the T^{ctp} crystals on the basis of screened precession photographs. Although these crystals actually diffracted better than the other forms, they could not be reproducibly grown. To produce the T_{pam} *P*321 crystals, we grew T-form crystals in the absence of PAM at pH 5.8 and then transferred the crystals to a buffer at pH 7.0 containing 20 mM PAM. Not only did these crystals diffract better than any of the other

forms, but because the space group is $P321$, we obtained two crystallographically independent views of the active site.

At either a pH near 6.0 or a pH near 7.0, we found that the combination of PAM with either L-aspartate, succinate, or L-malic acid resulted in crystals that had the same unit cell dimensions as T-state $P321$ or $R32$ crystals. The $R32$ T form grew most readily at pH 7.0 in the presence of PEG 8000, although we also found that the same crystal form would grow at pH 6.1–6.3 in the absence of PEG 8000. At pH 7.0, co-crystallization of PAM with any of the dicarboxylic acids mentioned above and adenosine triphosphate also yielded T-form $R32$ crystals. However, we found that the combination of PAM and malonate gave $P321$ R-state crystals at pH 5.8. When crystallization trials in the presence of these two ligands were attempted at higher pH, only precipitated protein resulted. However, by the addition of 20% (w/v) of PEG 8000 to the crystallization buffer, we were able to raise the pH of the buffer to as high as 7.8 without dissolving or cracking the crystals that were originally grown at pH 5.8.

Surprisingly, when T_{pam} crystals (pH 7.0) were transferred to a buffer containing 20 mM PAM and 8 mM malonate at pH 7.0, the allosteric transition from the T to the R state occurred in less than 24 h. The resultant crystals were still well ordered and diffracted to at least 3.0-Å resolution. Although some of the crystals subjected to these conditions developed cracks, many did not. When cracks appeared, they were circular in shape and located just inside the outside edge of the hexagonal plate. The outside rim of these cracked crystals could then be carefully removed from the rest of the crystal by using a small needle, leaving a circular plate that could be readily wedged into a capillary such that the thin dimension of the crystal was parallel to the long axis of the capillary.

Determination of PAM and Malonate Positions. In the T_{pam} structure the electron density associated with PAM was readily identified upon inspection of $F_o - F_c$ maps, where the F_cs and phases were calculated from only atoms contributed from the protein. The electron density peak defining the position of the phosphorus atom of the phosphonate group was the largest peak in the difference map. Placement of the amide group of PAM was also possible due to the ellipsoidal shape of the same peak evident at a lower contour level. The orientation of the plane of the amide group of PAM was partially determined by the somewhat flattened shape of the electron density at the tip of the ellipsoid and also by the position of hydrogen-bond donors and acceptors in the active site, as illustrated in Figure 3. All of the maps showing the electron density assigned to the ligands were computed by using phases and structure factors computed from the refined protein prior the inclusion of the ligands in the refinement. By doing this, we minimized the possibility of a "memory effect". In the $R_{pam,mal,crys}$ and $R_{pam,mal,soak}$ structures the placement of PAM relative to the protein atoms was similar to the placement of PAM in the T_{pam} structure as described above. However, determining the location of malonate was not as straightforward due to a weaker associated electron density peak. Nonetheless, it was possible to position malonate such that all of the atoms were associated with peaks in the electron density. These results are depicted in Figure 4.

We found that the electron density defining the positions of PAM and malonate in the $R_{pam,mal,crys}$ and the $R_{pam,mal,soak}$ structures was very similar. In fact, after least-squares superposition of the $R_{pam,mal,soak}$ structure onto the $R_{pam,mal,crys}$ structure using the method of Kabsch as employed by XPLOR, the rms difference in the positions of all non-hydrogen protein

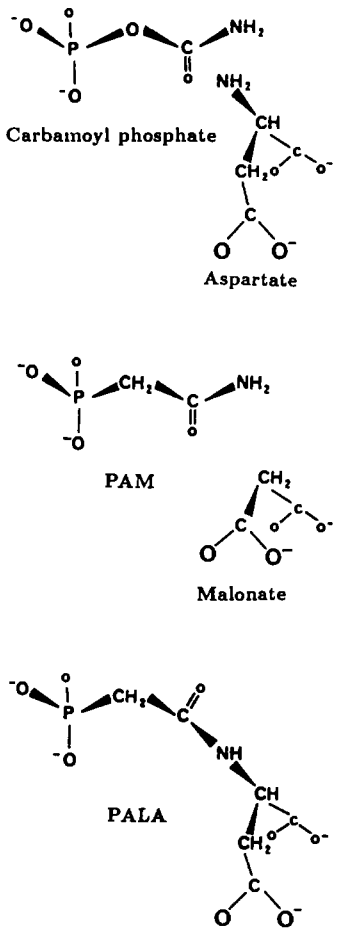

FIGURE 2: Chemical structures of the substrates, carbamoyl phosphate and aspartate, the bisubstrate analogue PALA, and the competitive inhibitors of carbamoyl phosphate and aspartate, phosphonoacetamide and malonate, respectively.

atoms was 0.19 Å. Since the two R-form structures reported here are essentially equivalent, and because the $R_{pam,mal,crys}$ structure is defined by more data, we used that structure to document the binding of PAM and malonate, and for comparisons with other structures. The smaller number of reflections in the $R_{pam,mal,soak}$ data set partially reflects the fact that those crystals were less well ordered than the $R_{pam,mal,crys}$ and also that the former data set was collected by using a shorter exposure time per frame.

Determination of Solvent Molecule Positions. Since the location of solvent at this moderate resolution is only possible for those solvent molecules that are as well ordered, in time and space, as some regions of the protein with the lowest mobility, we have only attempted to locate solvent, assumed to be water molecules, in and around the active site. In order for an electron density peak to be defined as a solvent molecule, we applied the criteria given in Ke et al. (1988). In addition, we note that except for the solvent located at the ligand sites, the solvent molecules built into both the T_{pam} and $R_{pam,mal}$ structures occupied similar positions in the T^{ctp} and R_{pala} structures, respectively. The binding of PAM to the T^{ctp} enzyme displaces water A393 in the C1 chain and water C358 in the C4 chain (Kim et al., 1987).

Conformational Changes Induced by the Binding of PAM. The alterations in the active site of aspartate carbamoyltransferase upon binding of PAM primarily involve the movement in the main-chain atoms of two sets of residues, Glu 50–Thr 55 and His 265–Asp 271, by as much as 1.8 Å and the movement of some of their side-chain groups by as much as 3.9 Å into the active site. To begin, we will consider the

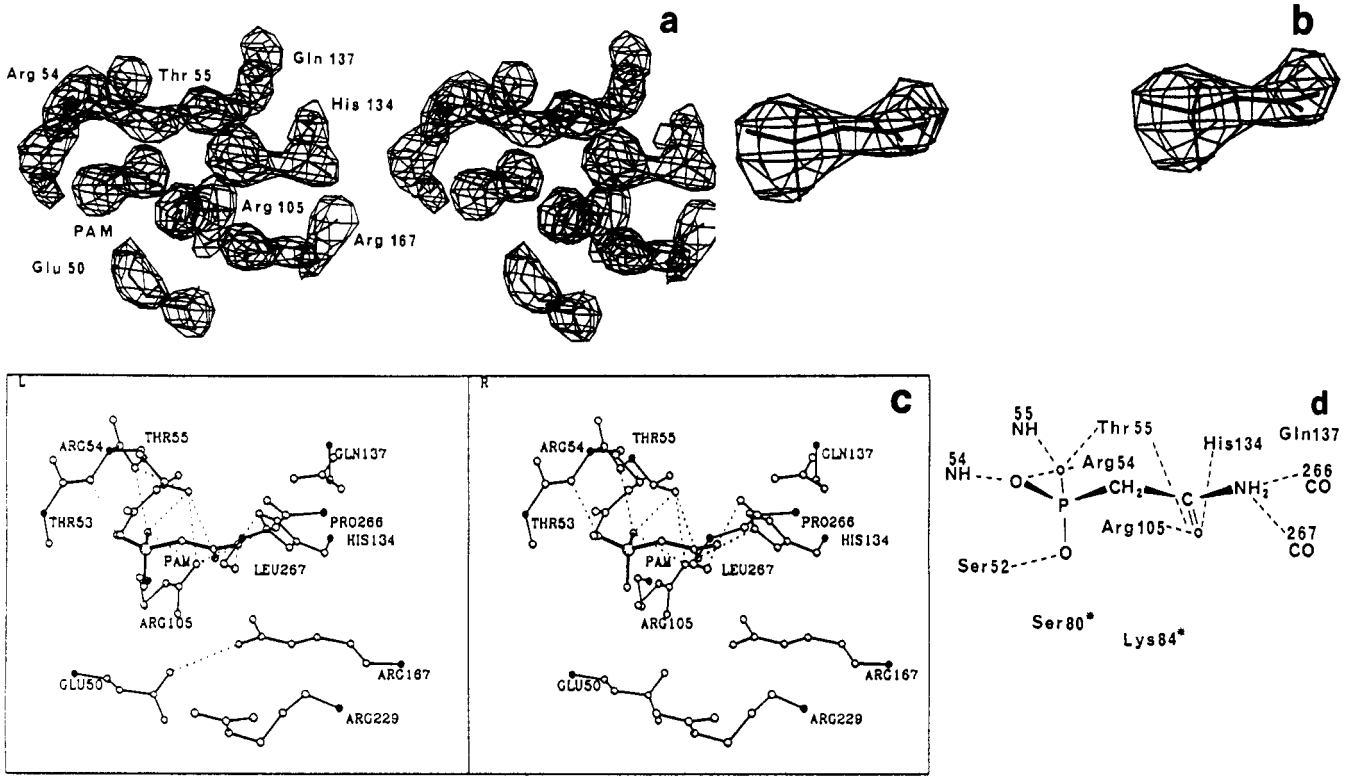

FIGURE 3: (a) Stereo drawing of an electron density map calculated by using the coefficients ($|F_o| - |F_c|$), where the F_cs and also the phases were calculated from the refined T_{pam} model with the residues Glu 50, Arg 54, Thr 55, Arg 105, Arg 167, and PAM omitted from the calculation. The map was contoured at 3σ. (b) Map computed in an analogous manner as the map in (a) except that here only PAM was omitted from the structure factor calculation. This map was contoured at 3.5σ. (c) Location of PAM in the active site shown by stereo drawing. Also indicated by dashed lines are possible salt links and hydrogen bonds between PAM and the active-site residues. (d) Schematic representation of the interactions between PAM and the enzyme. Ser 80 and Lys 84, donated from an adjacent chain, do not interact with PAM. See the text for a discussion of the binding of PAM to the C1 and C4 active sites.

first- and second-shell[2] contacts between the residues in the 50s region and PAM, as shown in Figures 3 and 5. One first-shell contact with PAM arises from Arg 54; its guanidinium group moves 1.4 Å from its position in the C1 chain of the T^{ctp} (Kim et al., 1987) structure to bind to the phosphonate of PAM. Coupled to the relocation of Arg 54 is the movement of Thr 55 by about 1.2 Å, also to its R-state position. The hydroxyl of Thr 55 interacts with both a phosphonate oxygen and the carbonyl oxygen of PAM. Near the methyl group of Thr 55, located in the interior of the carbamoyl phosphate domain, is the side chain of Phe 59. In the T^{ctp} structure the aromatic ring occupies at least two positions, related by a rotation around the $C_\alpha - C_\beta$ bond; the difference in the positions of CZ atoms on the aromatic ring is 2 Å, with one of the conformers positioning the ring closer to Thr 55. In the T_{pam} structure, Phe 59 occupies only the site that is farther from the methyl group of Thr 55 in the T^{ctp} structure. These conformational changes are illustrated in Figure 7.

On the other side of the active site from Arg 54, residues Pro 266–Pro 268 form a reverse turn in the polypeptide chain, defining the surface that recognizes the amino group of PAM (or carbamoyl phosphate). The larger segment of residues His 265–Asp 278 makes many important contacts with residues in the 240s loop and residues in an adjacent, 3-fold related catalytic chain. Upon ligation with PAM, the residues Pro 266–Pro 268 move up to 0.7 Å to a position near their R-state locations. This brings the adjacent residues, Arg 269–Asp 278, to a location intermediate between their T and R positions, as shown in Figure 8. The displacement of residues from Asp 271 through Asp 278 is coupled to the movement of Arg 269 by main-chain covalent bonds and by the salt link between the guanidinium group of Arg 269 and the carboxylate of Asp 278. In addition, the side chain of Arg 269 maintains its salt link with the carboxylate of Asp 90 from an adjacent, 3-fold related catalytic chain. Asp 276 is also linked to the end of the 240s loop by an interaction between the carboxylate of Asp 276 and the main-chain nitrogen of Ala 251. Although the residues in the 240s loop have moved little from their T-state positions in the T_{pam} structure, the first- and second-shell residues that lie between the 240s loop and the active site have shifted significantly toward their R-state position.

Glu 50 is a second-shell residue located in the carbamoyl phosphate domain that "switches" from an intradomain interaction with Arg 105 in the T^{ctp} structure to bind to Arg 167 and Arg 234 from the aspartate domain in the R state. In the C1 chain of the T_{pam} structure, the C_α of Glu 50 is 0.5 Å from its T^{ctp} location, approximately one-third of the way to its position in the $R_{pam,mal}$ structure; the carboxylate shifts 0.5 Å from the T^{ctp} structure to its position in the T_{pam} model, about halfway to its location in the R-state structure. These movements bring Glu 50 closer to Arg 167, as illustrated in Figure 9. Indeed, Arg 167, positioned on the opposite side of the active site and pointing toward Glu 50, has also moved farther into the active site such that its guanidinium group is 3.4 Å from the carboxylate of Glu 50, compared to a distance of 4.2 Å in the T^{ctp} structure.

[2] In an effort to develop a more precise vocabulary for discussing the interaction between ligands and macromolecules, we will call the direct interaction between the active-site residues and PAM *first shell* interactions; the residue in question will be defined as a first-shell residue. Likewise, an interaction between a residue that is not directly in contact with the ligand, but rather interacts with a first-shell residue, will be deemed a *second shell* interaction, and the residue will be called a second-shell residue.

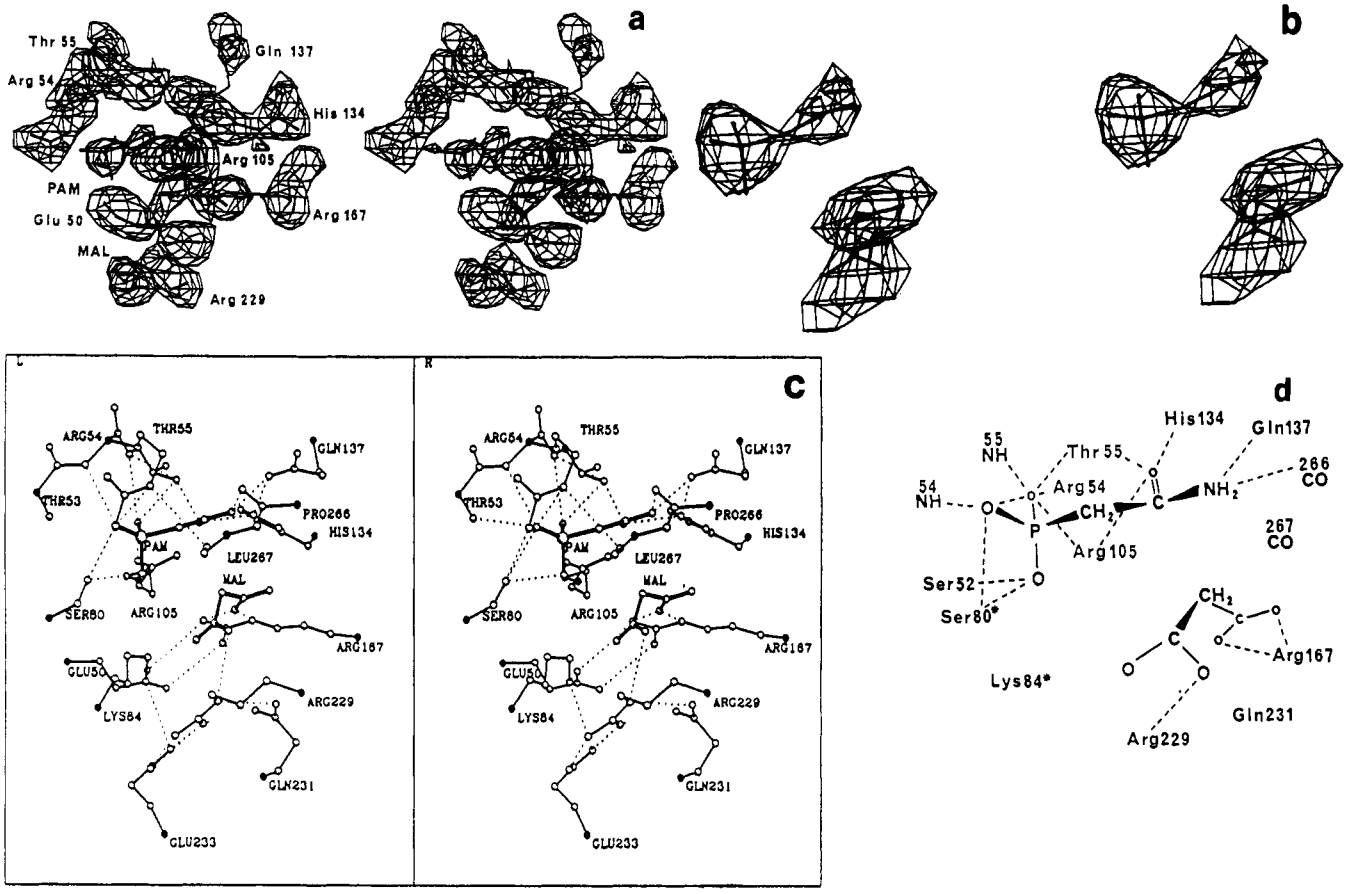

FIGURE 4: (a) Electron density map calculated by using the coefficients ($|F_o| - |F_c|$), where the F_cs and also the phases were computed from the $R_{pam,mal,crys}$ structure where the residues Glu 50, Arg 54, Thr 55, Arg 105, His 134, Gln 137, Arg 167, and Arg 229 and the ligands PAM and malonate were omitted from the computation. The map was contoured at 3.0σ. (b) Electron density associated with PAM and malonate, calculated analogously to the map in Figure 3b. (c) Location of PAM and malonate in the active site shown by stereo drawing. Possible salt links and hydrogen bonds are indicated by the dashed lines. The side-chain carbonyl oxygen of Gln 231 is close to the NH of the guanidinium group of Arg 229, but it is also close to its location in the PALA complex, where it makes a hydrogen bond to an oxygen of the β-carboxylate of PALA. The binding of PAM and malonate is very similar to the binding of carbamoyl phosphate and succinate (Gouaux & Lipscomb, 1988). (d) Schematic representation of the binding of PAM and malonate to the active site. Residues Ser 80 and Lys 84 reside on an adjacent, 3-fold related catalytic chain.

Although most of the differences between the T^{ctp} and the T_{pam} structures occur in both the lower and upper catalytic trimers (or C1 and C4 catalytic chains, respectively), the closure of the gap between C1 Glu 50 and C1 Arg 167 is not reproduced in the C4 chain. The distance of 5.0 Å between the side-chain groups of C4 Glu 50 and C4 Arg 167 in the T^{ctp} structure is maintained in the T_{pam} structure. To ensure that the crytallographically observed asymmetry in the Glu 50–Arg 167 interaction was not due to errors in the model, we swapped the catalytic chains of the final refined T_{pam} structure and re-refined the structure. This yielded a structure with a similar crystallographic residual and stereochemical quality and reproduced the asymmetry of the Glu 50–Arg 167 interaction noted in the first refined structure.

Conformational Changes Induced by the Binding of Malonate to the T_{pam} Enzyme. The binding of malonate to the PAM-ligated enzyme produces the same conformational changes that the binding of PALA induces (Ke et al., 1988). The interactions across the C1–C4, C1–R4, and C4–R1 interfaces that stabilize the T state of the enzyme are supplanted by new interactions between the substrate analogues and the enzyme and by interactions bridging the carbamoyl phosphate and aspartate domain interface. Some of these changes are illustrated and described in Figures 1 and 5. Upon malonate ligation of the T_{pam} enzyme, analogous to the binding of PALA to the unligated enzyme, we see the same dramatic movements of the 80s and 240s loops into the active site; this rearrangement brings residues Ser 80, Lys 84, Arg 229, and Gln 231 into contact with the ligands. The side chain of Arg 229 both binds to one of the carboxylates of malonate and interacts with the carboxylate of Glu 233. An interaction that further stabilizes the interface between the carbamoyl phosphate and aspartate domains occurs between the guanidinium moiety of Arg 234 and the carboxylate of Glu 50. The other carboxylate of malonate, located at the binding site of the α-carboxylate of PALA, interacts with Arg 167.

Comparison between the $R_{pam,mal,soak}$ and $R_{pam,mal,crys}$ Refined Structures. The structures of the two R-state PAM and malonate ligated enzymes, one determined from a crystal in which the T → R transition occurred within the crystal at pH 7.0 and the other where the crystals were grown in the presence of the ligands at pH 5.8 and subsequently transferred to a solution containing the ligands at pH 7.0, are identical at the current level of resolution, 2.8 Å. The rms over all non-hydrogen atom is 0.19 Å. Most importantly, the refined positions of the ligands and the positions of all the residues in the active sites are very similar.

Comparison between the Positions of Active-Site Residues of the $R_{pam,mal,crys}$ and R_{pala} Structures. The positions of all of the active-site residues in the PAM and malonate (pH 7.0) and PALA (pH 5.8) enzymes are similar except for the position of Lys 84. In the PALA-ligated enzyme the amino

FIGURE 5: (a) Location of the PAM binding site in a α-carbon stereo drawing of a catalytic monomer. Some of the important residues are illustrated. The 3-fold axis lies in the plane of the page and is approximately vertical. (b) Location of PAM and malonate in the $R_{pam,mal,crys}$ structure, in a drawing analogous to that in (a). Note the large movement of the 240s loop closer to the carbamoyl phosphate domain.

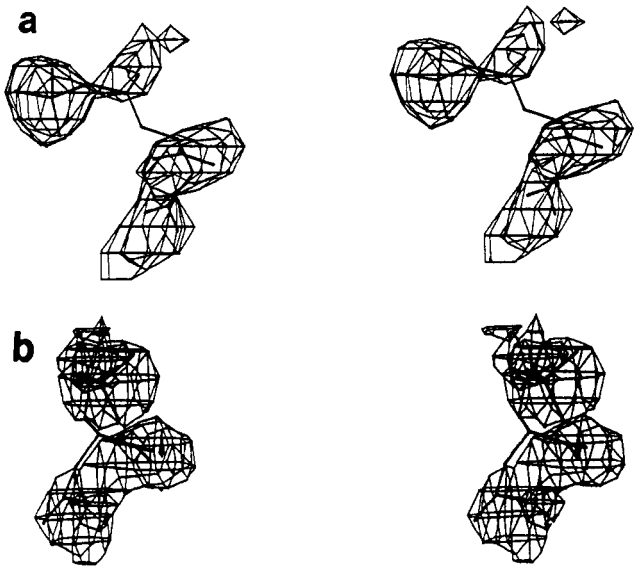

FIGURE 6: (a) Stereo drawing showing the position of PALA relative to the $R_{pam,mal,crys}$ electron density from Figure 4b. The coordinates of PALA were taken directly from the PALA–aspartate carbamoyltransferase refined structure, without any transformation. Note how well the phosphonoacetyl and carboxylates fit the density. (b) Another perspective of the same model and map, viewed down the carbon–phosphorus bond.

group of Lys 84 interacts with a phosphonate oxygen, an α-carboxylate oxygen, and a β-carboxylate oxygen. However, in both the $R_{pam,mal,crys}$ and $R_{pam,mal,soak}$ enzymes, the amino group of Lys 84 is 4.0 Å from the closest phosphonate oxygen of PAM and approximately 3.8 Å from a carboxylate oxygen. The amino group of Lys 84 in the PAM and malonate structures is within 3.3 Å of the carboxylate of Glu 233.

In fact, not only are the positions of PAM and malonate similar in the $R_{pam,mal}$ structures, but if the coordinates of PALA are extracted from the refined PALA–aspartate carbamoyltransferase structure without transformation, the phosphonoacetyl and carboxylate groups fit the PAM and malonate density from either the $R_{pam,mal,crys}$ or $R_{pam,mal,soak}$ structures very well. These results are illustrated in Figure 6.

Accuracy of the Coordinates. On the basis of multiple refinements of the T_{pam} structure starting from different sets of initial coordinates, we estimate the error in the coordinates for which there is strong electron density, such as the residues in the active site, to be approximately 0.5 Å. This value is similar to the estimated error derived from Luzzati plots (Luzzati, 1952). The differences between the structures discussed in this paper are equal to or greater than 0.5 Å.

Discussion

The CTP-ligated T-state (T^{ctp}) structure served as an excellent molecular replacement model for the solution of the T_{pam} structure, even though the T^{ctp} structure was determined in the presence of different ligands and at a different pH. Indeed, Schachman, Kim, and co-workers have calculated difference maps at pH 7.0 using the observed intensities from one crystallized mutant of aspartate carbamoyltransferase (Komiya et al., 1985; Komiya, 1987) and have partially refined the structure of another mutant (Young, 1984; Lu et al., 1988) by utilizing the coordinates and phases of the *R*32 or *P*321 T-state crystal forms, as determined in this laboratory (Ke et al., 1984; Honzatko & Lipscomb, 1982; Monaco et al., 1978; Warren et al., 1973; Wiley et al., 1971). Equally effective in providing starting points for the determination of the PAM and malonate R-state structures were the coordinates and

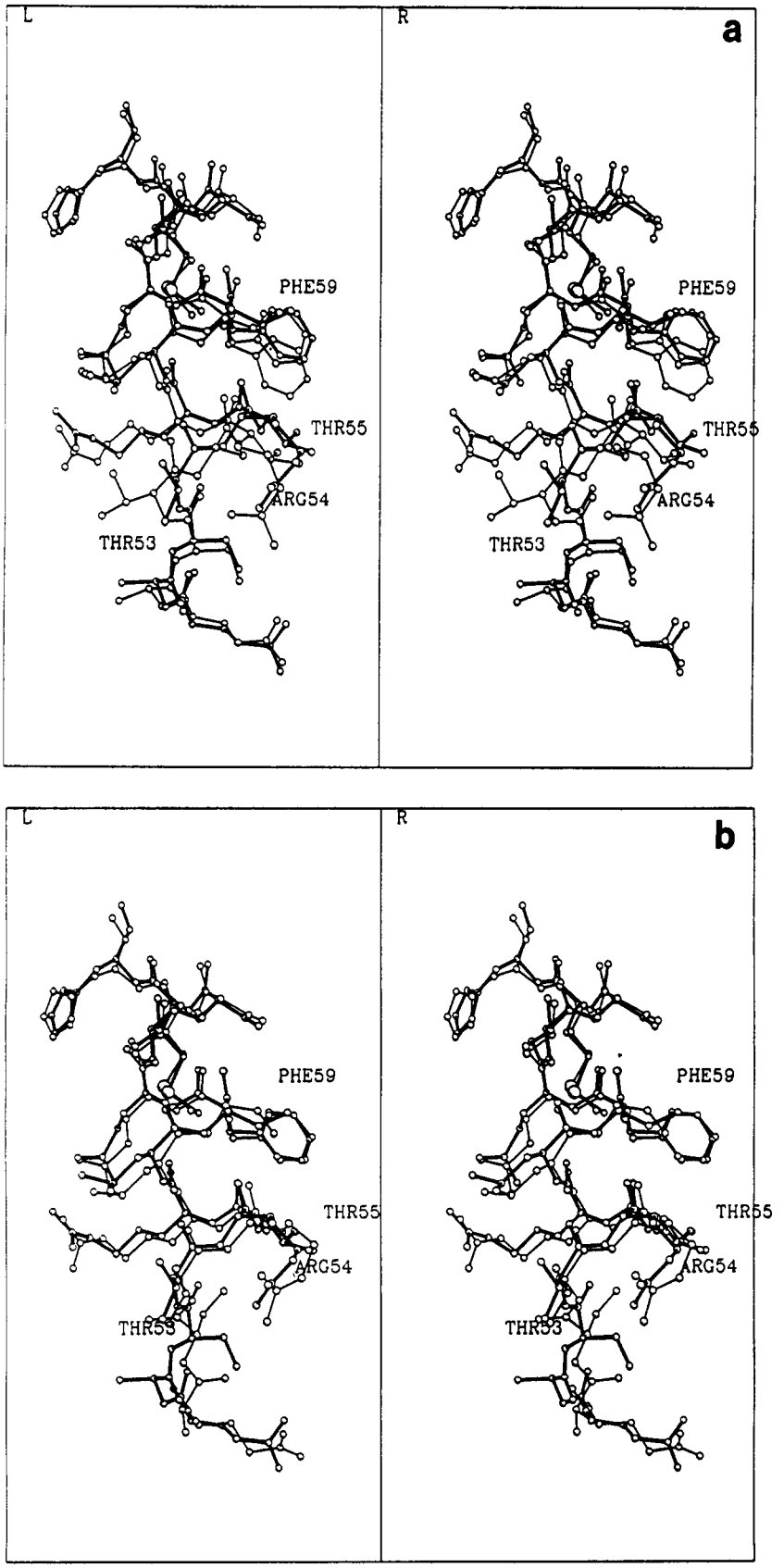

FIGURE 7: (a) Residues Glu 50–His 64 of the T_{pam} structure drawn in thick filled lines superimposed on the same residues of the T^{ctp} structure drawn in thin lines. The residues Thr 53–Thr 55 have moved to their R-state positions in the T_{pam} structure and Phe 59 occupies only one of the two T^{ctp} conformations. (b) Superimposed in this drawing are Glu 55–His 64 from the T_{pam} and $R_{pam,mal,crys}$ structures. All of the residues are in similar positions except for the region around Ser 52.

phases originally obtained from the PALA-ligated R-state structure, also determined in this laboratory (Ke et al., 1988; Krause et al., 1985, 1987; Ladner et al., 1982). These well-determined structures combined with the powerful molecular dynamics and Powell minimization methods as incorporated into XPLOR, running on the supercomputers at the Pittsburgh Supercomputer Center, enabled the refinement of the structures reported here to proceed rapidly.

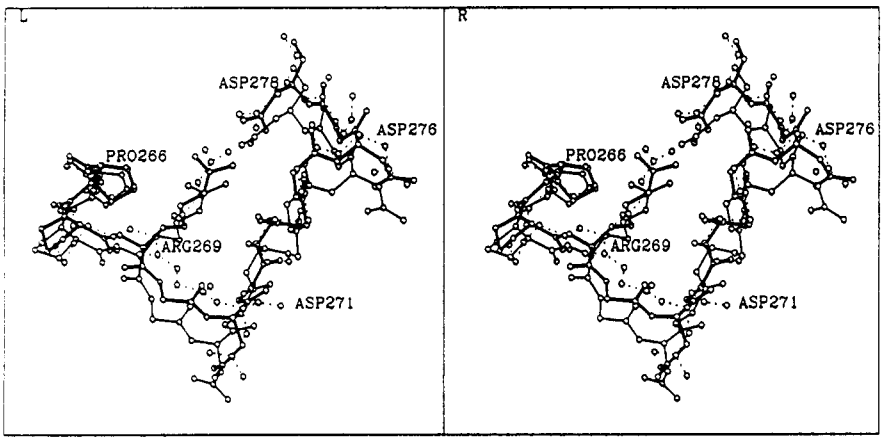

FIGURE 8: Represented in this stereo drawing are the T_{pam} (thick lines) and $R_{pam,mal,crys}$ (thin lines) regions from Pro 266 to Asp 278 superimposed on the same region from the T^{ctp} structure (dashed lines).

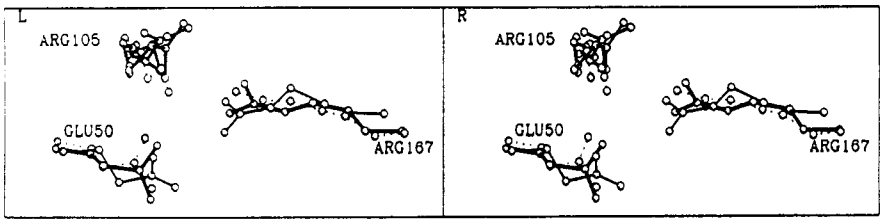

FIGURE 9: Stereo drawing of the residues Glu 50, Arg 105, and Arg 167 from the T^{ctp} (dashed lines), T_{pam} (thick lines), and $R_{pam,mal,crys}$ structures.

Nonetheless, the behavior of aspartate carbamoyltransferase in solution is dependent upon pH (Pastra-Landris et al., 1978). Since the paradigm T- and R-state crystal structures of the enzyme were determined at a pH near 5.8 where the enzyme exhibits very low activity and cooperativity, we decided to determine the structures of ligated forms of the enzyme at pH 7.0. Important as the difference in pH from 5.8 to 7.0 is for the enzyme's function, it has previously been documented that the quaternary T and R structures of the enzyme, as determined from the crystallographic studies at pH 5.8, are similar to the quaternary structures of the enzyme at pH 8.3 in solution (Altman et al., 1982) on the basis of low-angle X-ray scattering measurements (Moody et al., 1979). Indeed, the ultraviolet difference spectra obtained upon carbamoyl phosphate ligation for the catalytic trimer were also shown to be essentially invariant over the pH range 6.0–8.5 (Lauritzen & Lipscomb, 1980). Consequently, the pH dependence of the function of aspartate carbamoyltransferase might manifest itself in structurally somewhat subtle conformational rearrangements, but not by large changes in tertiary or quaternary structure.

One difference in the T^{ctp} (pH 5.8) and T_{pam} (pH 7.0) structures that might be related to the variation in homotropic and heterotropic cooperativity as a function of pH is the interaction between Asp 236 in the catalytic chain and Lys 143 in the regulatory chain; in the T state these residues form part of the C1–R4 interface, an interface not present in the R state. In the T_{pam} structure the side-chain groups of Asp 236 and Lys 143 are separated by 3.4 and 3.8 Å in the C1–R4 and C4–R1 interfaces, respectively. In the T^{ctp} structure, the analogous distances are 4.1 (C1–R4) and 4.6 Å (C4–R1). We suggest that the importance of these residues in communicating heterotropic and homotropic information be tested by site-directed mutagenesis.

As indicated in Table III, the pH did not affect the quaternary state induced by the cocrystallization of the enzyme with PAM alone or with PAM plus L-aspartate, L-malic acid, or succinate on the basis of the crystals' unit cell dimensions. Because one of the goals of these experiments was to find a combination of stable ligands that would induce the T → R transition, we turned to the combination of PAM and malonate. The crystallization experiments, combined with the fact that PAM and malonate are competitive inhibitors of carbamoyl phosphate and aspartate, respectively (Porter et al., 1969), indicated that they would be useful substrate analogues to employ in our crystallographic studies.

To perform the crystallographic studies at a higher pH, we transferred T-state *P*321 crystals to a buffer containing 20 mM PAM and 15% (w/v) PEG 8000 at pH 7.0. The hexagonal plates were stable for more than 4 months under these conditions. Most importantly, we discovered that if these PAM-ligated T-state crystals, at pH 7.0, were moved to a buffer containing both PAM and malonate at pH 7.0, the crystals transformed to single *P*321 crystals that had the same unit cell dimensions as the PAM and malonate ligated R-state crystals that were grown at pH 5.8. As a result of this transformation, the *c*-axis unit cell dimension increased by 14 Å. Although subsequent experiments indicated that the transformation does not proceed via a simultaneous isomerization of all of the molecules, there might be some degree of cooperativity between molecules or between planes of molecules. Interactions between molecules might be important factors in preserving the long-range order of the crystal.

The largest conformational change that occurs upon the binding of PAM to the T-state enzyme is the relocation of the 50s loop to its R-state position, as illustrated in Figure 7. Listed in Table IV are the possible hydrogen bonds and salt links that PAM makes with the enzyme. In addition to forming a salt link to PAM, the side chain of Arg 54 makes a second-shell ion pair interaction with the carboxylate of Glu 86, a residue from an adjacent, 3-fold related catalytic chain contained in the same trimer. Glu 86 acts as a tether for the 80s loop, a flexible region that moves backbone atoms up to 5.0 Å into the active site as a result of the T → R transition. This movement of the 80s loop is essential for contact of Lys 84 with aspartate and carbamoyl phosphate: Lys 84 makes

Table IV: Possible Hydrogen Bonds between PAM and Active-Site Residues

PAM atom[a]	protein atom[b]	distance[c] (Å)	angle[c] (deg)
OP1	Ser 52 OG	3.0/2.7	117/151
OP2	Arg 54 NH	2.7/2.9	120/147
OP2	Arg 54 NH2	3.3/3.1	153/135
OP3	Thr 55 NH	2.9/2.6	151/131
OP3	Thr 55 OG1	2.7/2.6	141/111
O1	Thr 55 OG1	3.2/3.3	128/107
O1	Arg 105 NH1	2.9/3.0	154/137
O1	His 134 NE2[d]	3.1/3.7	128/-
N1	Gln 137 OE1[d]	3.6/3.3	-/101
N1	Pro 266O[d]	3.3/4.0	128/-
N1	Pro 267O[d]	3.1/4.0	133/-

[a] Atoms OP1, OP2, and OP3 are the phosphonate oxygens, and atoms O1 and N1 are the carbonyl oxygen and primary amino nitrogen, respectively. [b] The distances and angles between the atoms in the lower or C1 active site are given first, and the distances and angles between the atoms in the upper or C4 active site are listed second. [c] This is a list of the interactions between the polar atoms that are within 3.4 Å and where the angles defined by the PAM atom, hydrogen, and protein atom are greater than 90°. The positions of the hydrogen atoms were determined in the course of the protein refinement by the computer program XPLOR. [d] Interactions between the primary amide group of PAM and the active-site residues differ significantly in the C1 and C4 active sites. However, the interactions between the phosphonate groups and the active-site residues are similar in both active sites.

Table V: Interactions between PAM and Malonate and Active-Site Residues

ligand atom[a]	protein atom[b]	distance[c] (Å)	angle[c] (deg)
PAM OP1	Ser 80[d] OG	3.5/3.1	81/123
PAM OP1	Lys 84[d] NZ	4.0/4.0	-/-
PAM OP1	Arg 105 NH1	3.4/2.9	100/116
PAM OP2	Thr 53 NH	3.2/3.1	143/154
PAM OP2	Arg 54 NH	3.0/2.7	135/142
PAM OP2	Arg 54 NH1	3.0/3.3	110/110
PAM OP2	Arg 54 NE	3.3/3.3	105/111
PAM OP3	Ser 52 OG	2.7/2.5	123/114
PAM OP3	Thr 55 NH	3.1/2.8	162/158
PAM OP3	Thr 55 OG1	3.1/2.9	143/152
PAM OP3	Arg 105 NH1	2.6/2.9	130/137
PAM O1	Thr 55 OG1	2.8/2.9	133/126
PAM O1	Arg 105 NH2	3.5/3.3	105/158
PAM O1	His 134 NE2	3.1/3.0	112/130
PAM N1	Gln 137 OE2	2.6/3.1	133/119
PAM N1	Pro 266 O	3.4/3.6	172/152
PAM N1	Leu 267 O	3.6/3.3	124/137
MAL O1	Arg 229 NE	3.2/3.3	133/161
MAL O1	Gln 231 NE2	3.1/3.0	158/156
MAL O2	Arg 229 NE	3.6/3.1	131/120
MAL O2	Arg 229 NH1	3.1/2.7	128/127
MAL O3	Arg 167 NH2	2.5/3.0	111/122

[a] Atoms OP1, OP2, and OP3 are the phosphonate oxygens, and atoms O1 and N1 correspond to the carbonyl oxygen and primary amino nitrogen, respectively. [b] The distances and angles between the atoms in the lower or C1 active site are the first numbers in each pair, and the distances and angles between the atoms in the upper or C4 active site are the second numbers in each pair. [c] This is a list of some of polar interactions between ligand atoms and protein atoms. The angular values refer to the hydrogen-bond angle for those atoms within 3.8 Å. The positions of the hydrogen atoms were determined in the course of the protein refinement by the computer program XPLOR. [d] These residues are donated from an adjacent, 3-fold related catalytic chain.

first-shell contacts with the phosphate group of carbamoyl phosphate and the carboxylate of succinate in the R state (Gouaux & Lipscomb, 1988). Chemical modification (Kempe & Stark, 1975; Lauritzen & Lipscomb, 1982) and site-directed mutagenesis (Robey et al., 1986) studies have shown that Lys 84 is critical for activity. These experiments support the crystallographic results (Krause et al., 1985) which first indicated that the active site is shared between adjacent catalytic monomers of the catalytic trimers of aspartate carbamoyltransferase. Throughout the T → R transition Arg 54 maintains a salt link with Glu 86, possibly as mechanism for guiding the 80s loop into and out of the active site. However, in the T_{pam} structure neither Lys 83 nor Lys 84 has moved into the active site to make direct contact with PAM.

In the Arg 54 → Ala mutant[3] the K_D for the binding of carbamoyl phosphate to both the holoenzyme and the catalytic trimer is greater by more than a factor of 10, as measured by circular dichroism and kinetic experiments (Stebbins et al., 1989). However, the catalytic activities of the mutant holoenzyme and catalytic trimer are reduced by factors of 17000 and 70000, respectively. This information, in conjunction with some of the crystallographic information presented here, might lead one to conclude that Arg 54 is a catalytically important residue. Yet if the interaction between Arg 54 and Glu 86 helps to position the end of the 80s loop—the region of residues near Lys 84—then another explanation for the low catalytic activity of the Arg 54 → Ala mutant might be that the mutation precludes the optimal interaction between Lys 84 and the substrates and reactive intermediates. Of course, the reduced activity of the Arg 54 → Ala mutant is probably due to a number of factors that impact both the correct binding of substrates and the catalysis of the chemical reaction.

Experiments carried out in solution probing the binding of carbamoyl phosphate and some of its analogues to the holoenzyme in the absence of the aspartate analogue succinate have indicated that there are three tight sites and three weak sites, where the binding constants differ by about a factor of 20 (Suter & Rosenbusch, 1976). The crystallographic results from the T_{pam} structure indicate that a structural basis for the native cooperativity of carbamoyl phosphate binding might be due, at least in part, to the presence or absence of a salt link between Glu 50 and Arg 167, as shown in Figure 9. Since the movement of Arg 167 is coupled to the 240s loop of the other catalytic trimer, through the interaction of Lys 164 (C1) and Tyr 165 (C1) with Glu 239 (C4) across the C1–C4 interface, the holoenzyme can accommodate the movement of only three of the Arg 167s toward their R-state positions while maintaining the T quaternary structure. Intermolecular contacts in the crystal also might be partly responsible for rendering the active sites in the C1 and C4 catalytic chains asymmetric.

In the T_{pam} and $R_{pam,mal}$ structures, the binding of PAM's amide group is significantly different. The NH_2 group of PAM binds to the main-chain carbonyl oxygens of Pro 266 and Leu 267 in the C1 active site and it interacts with only the side-chain carbonyl oxygen of Gln 137 in the C4 active site of the T_{pam} structure. However, in both of the crystallographically independent active sites in the R-state structures, the NH_2 group of PAM is closest to the side-chain oxygen of Gln 137. These results complement the experiments which showed that the Gln 137 → Ala mutant exhibits a reduced affinity for carbamoyl phosphate (Stebbins et al., 1989). It is structurally plausible that the main-chain carbonyl oxygen of Leu 267, which interacts with the amino group of PALA (Krause et al., 1987), could interact with the amino group aspartate and the carbonyl oxygen of Pro 266, and the side-chain carbonyl oxygen of Gln 137 could accept hydrogen bonds from the amino group of carbamoyl phosphate.

Another consequence of the binding of PAM to the T-state enzyme is that a number of first- and second-shell residues

[3] The notation we use to name a mutant enzyme consists of the wild-type amino acid followed by its numerical location in the sequence on the left of an arrow, and on the right of the arrow is the abbreviation of the new amino acid. For example, Arg 54 → Ala indicates that the arginine at position 54 was changed to an alanine.

which exist in more than one conformation in the T^{ctp} structure adopt only one conformation in the T_{pam} structure. For example, in the C4 chain of the T^{ctp} structure, Arg 54 occupies two conformations. In one conformation the guanidinium group interacts with the hydroxyl oxygen of Tyr 98 from an adjacent chain, and in the other conformation the side-chain group is bound to the carboxylate of Glu 86, also from an adjacent catalytic chain (Kim et al., 1987). In both of the catalytic chains of the T_{pam} structure, Arg 54 exists only in the conformation where its side chain interacts with Glu 86. When in this conformation, the guanidinium group can also interact with the phosphonate of PAM.

A second-shell residue that occupies two distinct conformations in the T^{ctp} structure (Kim et al., 1987) and only one conformation in the T_{pam} structure is Phe 59. This residue, located on the second helix of the catalytic chain and just above Thr 55, is oriented with its side chain in the interior of the carbamoyl phosphate domain, as illustrated in Figure 7. In the T^{ctp} structure, one of the conformations of the phenyl ring places it closer (3.8 Å) to the Thr 55 methyl group than does the other conformation (5.5 Å). Upon ligation of the enzyme with PAM, the phenyl ring occupies only the conformation that is farther from the methyl group of Thr 55 in the T^{ctp} structure; if the phenyl ring occupied the alternate conformation of the T^{ctp} structure, the ring would collide with the methyl group of Thr 55. We speculate that Arg 54, Thr 55, and Phe 59 adopt more than one conformation to facilitate substrate binding and product release.

With respect to the catalytic mechanism, the T_{pam} and $R_{pam,mal}$ structures corroborate the previous crystallographic studies on the binding of phosphate and pyrophosphate (Honzatko & Lipscomb, 1982) to the T-state enzyme, the binding of PALA (Volz et al., 1986), carbamoyl phosphate, and succinate to the R-state enzyme (Gouaux & Lipscomb, 1988), and the molecular modeling of a hypothetical tetrahedral intermediate (Gouaux et al., 1987) also to the R-state enzyme. Nuclear magnetic resonance (NMR) studies indicated that the carbonyls of PALA and carbamoyl phosphate (in the presence of succinate) are hydrogen bonded to a residue, or residues, in the active site (Roberts et al., 1976). This type of interaction might render the carbonyl carbon of carbamoyl phosphate more susceptible to nucleophilic reaction by aspartate. In the $R_{pam,mal,crys}$ structure we find that the carbonyl oxygen of PAM can accept hydrogen bonds from Thr 55, Arg 105, and His 134. Although a catalytic role has been proposed for His 134, the His 134 → Ala mutant is nonetheless 5% as active as the wild-type enzyme, indicating that His 134 is important but not essential for catalysis (Robey et al., 1986); the interpretation of subsequent NMR experiments on the His 134 → Ala mutant and native catalytic trimers was that His 134 did not act as either a general acid or a general base (Kleanthous et al., 1988). Gln 137, which binds to the primary amino group of a hypothetical tetrahedral intermediate (Gouaux et al., 1987), the NH_2 group of carbamoyl phosphate (Cherfils, 1986; Gouaux & Lipscomb, 1988), and the NH_2 of PAM, probably also will interact with the NH_2 of *N*-carbamoyl-L-aspartate. The interactions of Gln 137 with carbamoyl phosphate might distort the carbamoyl moiety from planarity, thereby destabilizing the substrate and rendering carbamoyl phosphate more susceptible to reaction with aspartate (Gouaux & Lipscomb, 1988). Following the attack of the amino group of aspartate, it is structurally possible that a phosphate oxygen deprotonates aspartate's positively charged NH_2 group, thereby catalyzing the decomposition of the tetrahedral intermediate (Gouaux et al., 1987).

Since the binding of PAM to the T-state enzyme induces some of the same conformational changes that the binding of phosphate induces (Honzatko & Lipscomb, 1982; Gouaux and Lipscomb, unpublished results), experiments performed in phosphate buffer probe the behavior of the phosphate-ligated enzyme. We have shown that phosphate, in combination with aspartate, can transform T crystals to crystals with a *c*-axis unit cell dimension that is intermediate between the T and R *c*-axis unit cell dimensions (Gouaux & Lipscomb, 1989a). Consequently, studies such as the sedimentation experiments performed on the Asn 111 → Ala regulatory chain mutant enzyme in 40 mM phosphate buffer (Eisenstein et al., 1989) determined the sedimentation properties of the phosphate-ligated enzyme and not the unligated enzyme. Indeed, if a mutation sufficiently destabilizes the T state, the binding of an active-site ligand such as phosphate might be able to promote the T → R transition. In fact, phosphate binds at 20 mM to the native enzyme in the crystalline state (Honzatko & Lipscomb, 1982).

On the basis of the enzyme–substrate analogue structures described here, we can formulate a stereochemical mechanism for the initial steps in the allosteric transition. First, carbamoyl phosphate binds tightly to three of the six active sites, shifting Arg 54, the 50s loop, and residues 266–268 to their R-state positions. Associated with this isomerization is a small movement of second- and third-shell residues in the 80s and 240s loops toward their R-state conformations. In half of the active sites, Glu 50 and Arg 167 have moved toward each other to form a salt link while the separation between Glu 50 and Arg 105 has increased, allowing Arg 105 to bind to carbamoyl phosphate. The formation of the interdomain ion pair between Glu 50 and Arg 167 is the first of many interactions that are important for stabilizing the R state. In the three other active sites, Glu 50 remains near Arg 105 and Arg 167 stays in its T^{ctp} position. Although many facets of the structural and functional behavior of aspartate carbamoyltransferase are consistent with the model of Monod et al. (1965), the sequential model of Koshland et al. (1966) is more consistent with these early conformational changes associated with the binding of PAM, and by extension by binding of carbamoyl phosphate, to the holoenzyme.

We note that the early conformational changes on the T → R pathway are in the comparatively rigid loops that form much of the active site and make many primary shell interactions with phosphonoacetamide; the movement of the atoms in these regions is coupled to other more flexible loops that undergo large conformational changes upon the binding of aspartate. Although the coupling of the movement between these regions occurs through many different interactions, one of the most obvious mechanisms is the enzyme's use of salt links and hydrogen bonds. The importance of these obvious mechanisms in transmitting conformational information can be further elucidated through a combination of structural, functional, and mutagenesis experiments. Besides these studies, we also expect to study the mechanism for the binding of aspartate and the relationship of that event to T → R transition and chemical catalysis.

Acknowledgments

We thank R. H. Kretsinger, S. Sobottka, R. Chandros, and T. Ptak for the use of the Biotechnology Resource at the University of Virginia for collection of the X-ray diffraction data. We appreciate the help of Axel Brünger in setting up XPLOR on the CRAY YMP at the Pittsburgh Supercomputer Center (PSC). We thank John F. Stanton for performing the INDO calculations. Use of the CRAY YMP at the PSC has

tremendously increased the progress of this study and is gratefully acknowledged.

Registry No. Phosphonoacetamide, 22363-89-9; diethylphosphonoacetamide, 5464-68-6; disilylphosphonoacetamide, 123933-44-8.

REFERENCES

Altman, R. B., Ladner, J. E., & Lipscomb, W. N. (1982) *Biochem. Biophys. Res. Commun. 108*, 592–595.

Balsiger, R. W., Jones, D. G., & Montgomery, J. A. (1959) *J. Org. Chem. 24*, 434–436.

Brünger, A. T. (1988) *XPLOR Manual*, version 1.5.

Brünger, A. T., Kuriyan, J., & Karplus, M. (1987) *Science 235*, 458–460.

Butler, K. R., & Snow, M. R. (1976) *J. Chem. Soc., Dalton Trans.*, 251.

Cherfils, J. (1987) Dissertation, Universite Paris-Sud, Orsay, France.

Collins, K. D., & Stark, G. R. (1969) *J. Biol. Chem. 244*, 1869–1877.

Colman, P. D., & Markus, G. (1972) *J. Biol. Chem. 247*, 3829–3837.

Eisenstein, E., Markby, D. W., & Schachman, H. K. (1989) *Proc. Natl. Acad. Sci. U.S.A. 86*, 3094–3098.

Fox, G. C., & Holmes, K. C. (1966) *Acta Crystallogr. 20*, 886–891.

Gerhart, J. C., & Schachman, H. K. (1968) *Biochemistry 7*, 538–552.

Gouaux, J. E., & Lipscomb, W. N. (1988) *Proc. Natl. Acad. Sci. U.S.A. 85*, 4205–4208.

Gouaux, J. E., & Lipscomb, W. N. (1989a) *Proc. Natl. Acad. Sci. U.S.A. 86*, 845–848.

Gouaux, J. E., & Lipscomb, W. N. (1989b) *Biochemistry 28*, 1798–1803.

Gouaux, J. E., Krause, K. L., & Lipscomb, W. N. (1987) *Biochem. Biophys. Res. Commun. 142*, 893–897.

Griffin, J. H., Rosenbusch, J. P., Weber, K. K., & Blout, E. R. (1972) *J. Biol. Chem. 247*, 6482–6490.

Griffin, J. H., Rosenbusch, J. P., Weber, K. K., & Blout, E. R. (1973) *J. Biol. Chem. 248*, 5057–5062.

Honzatko, R. B. (1986) *Acta Crystallogr. A42*, 172–178.

Honzatko, R. B., & Lipscomb, W. N. (1982) *J. Mol. Biol. 160*, 265–286.

Howlett, G. J., Blackburn, M. N., Compton, J. G., & Schachman, H. K. (1977) *Biochemistry 16*, 5091–5099.

Hsuanyu, Y., & Wedler, F. C. (1987) *Arch. Biochem. Biophys. 259*, 316–330.

Jacobson, G. R., & Stark, G. R. (1975) *J. Biol. Chem. 250*, 6852–6860.

Jones, M. E., Spector, L., & Lipmann, F. (1955) *J. Am. Chem. Soc. 77*, 819–820.

Jones, T. A. (1982) in *Computational Crystallography* (Sayre, D., Ed.) pp 303–317, Oxford, U.K.

Kabsch, W. (1976) *Acta Crystallogr. A32*, 922–923.

Kantrowitz, E. R., & Lipscomb, W. N. (1988) *Science 241*, 669–674.

Ke, H.-M., Honzatko, R. B., & Lipscomb, W. N. (1984) *Proc. Natl. Acad. Sci. U.S.A. 81*, 4037–4040.

Ke, H.-M., Lipscomb, W. N., Cho, Y., & Honzatko, R. B. (1988) *J. Mol. Biol. 204*, 725–747.

Kempe, T. D., & Stark, G. R. (1975) *J. Biol. Chem. 250*, 6861–6869.

Kim, K. H., Pan, Z., Honzatko, R. B., Ke, H.-M., & Lipscomb, W. N. (1987) *J. Mol. Biol. 196*, 853–875.

Kleanthous, C., Wemmer, D. E., & Schachman, H. K. (1988) *J. Biol. Chem. 263*, 13062–13067.

Komiya, H. (1987) Dissertation, University of California, Berkeley, CA.

Komiya, H., Schachman, H. K., & Kim, S.-H. (1985) Abstract from the American Crystallographic Association Meeting, Aug 18–29, Stanford University, Stanford, CA.

Koshland, D. E., Némethy, G., & Filmer, D. (1966) *Biochemistry 5*, 365–385.

Krause, K. L., Volz, K. W., & Lipscomb, W. N. (1985) *Proc. Natl. Acad. Sci. U.S.A. 82*, 1643–1647.

Krause, K. L., Volz, K. W., & Lipscomb, W. N. (1987) *J. Mol. Biol. 193*, 527–553.

Ladner, J. E., Kitchell, J. P., Honzatko, R. B., Ke, H.-M., Volz, K. W., Kalb (Gilboa), A. J., Ladner, R. C., & Lipscomb, W. N. (1982) *Proc. Natl. Acad. Sci. U.S.A. 79*, 3125–3128.

Lauritzen, A. M., & Lipscomb, W. N. (1980) *Biochem. Biophys. Res. Commun. 95*, 1425–1430.

Lauritzen, A. M., & Lipscomb, W. N. (1982) *J. Biol. Chem. 257*, 1312–1319.

Lu, T. H., Young, T. S., Schachman, H., & Kim, S.-H. (1988) *J. Chin. Chem. Soc. 35*, 315–319.

Luzzati, V. (1952) *Acta Crystallogr. 5*, 802–810.

Manojlović, L., & Speakman, J. C. (1967) *J. Chem. Soc. A*, 971–979.

Monaco, H. L. (1978) Dissertation, Harvard University, Cambridge, MA.

Monaco, H. L., Crawford, J. L., & Lipscomb, W. N. (1978) *Proc. Natl. Acad. Sci. U.S.A. 75*, 5276–5280.

Monod, J., Wyman, J., & Changeux, J.-P. (1965) *J. Mol. Biol. 12*, 88–118.

Moody, M. F., Vachette, P., & Foote, A. M. (1979) *J. Mol. Biol. 133*, 517–532.

Nowlan, S. F., & Kantrowitz, E. R. (1985) *J. Biol. Chem. 260*, 14712–14716.

Pastra-Landis, S. C., Evans, D. R., & Lipscomb, W. N. (1978) *J. Biol. Chem. 253*, 4624–4630.

Pflugrath, J. W., Saper, M. A., & Quiocho, F. A. (1984) in *Methods and Applications in Crystallographic Computing* (Hall, S., & Ashiaka, T., Eds.) pp 404–407, Clarendon Press, Oxford, U.K.

Phillips, J. C., Bordas, J., Foote, A. M., Koch, M. H. J., & Moody, M. F. (1982) *Biochemistry 21*, 830–834.

Porter, R. W., Modebe, M. O., & Stark, G. R. (1969) *J. Biol. Chem. 244*, 1846–1859.

Reichard, P., & Hanshoff, G. (1956) *Acta Chim. Scand. 10*, 548–566.

Roberts, M. F., Opella, S. J., Schaffer, M. H., Phillips, H. M., & Stark, G. R. (1976) *J. Biol. Chem. 251*, 5976–5985.

Robey, E. A., Wente, S. R., Markby, D. W., Flint, A., Yang, Y. R., & Schachman, H. K. (1986) *Proc. Natl. Acad. Sci. U.S.A. 83*, 5934–5938.

Sobottka, S. E., Cornick, G. G., Kretsinger, R. H., Rains, R. G., Stephens, W. A., & Weissman, L. J. (1984) *Nucl. Instrum. Methods 220*, 575–581.

Stebbins, J. W., Xu, W., & Kantrowitz, E. R. (1989) *Biochemistry 28*, 2592–2600.

Suter, P., & Rosenbusch, J. P. (1976) *J. Biol. Chem. 251*, 5986–5991.

Swenson, D., Baenziger, N. C., & Coucouvanis, D. (1978) *J. Am. Chem. Soc. 100*, 1932–1934.

Volz, K. W., Krause, K. L., & Lipscomb, W. N. (1986) *Biochem. Biophys. Res. Commun. 136*, 822–826.

Warren, S. G., Edwards, B. F. P., Evans, D. R., Wiley, D. C., & Lipscomb, W. N. (1973) *Proc. Natl. Acad. Sci. U.S.A. 70*, 1117–1121.

Wedler, F. C., & Gasser, F. J. (1974) *Arch. Biochem. Biophys. 163*, 57-68.
Wiley, D. C., & Lipscomb, W. N. (1968) *Nature 218*, 1119-1121.
Wiley, D. C., Evans, D. R., Warren, S. G., McMurray, C. H., Edwards, B. F. P., Franks, W. A., & Lipscomb, W. N. (1971) *Cold Spring Harbor Symp. Quant. Biol. 36*, 285-290.
Young, T.-S. (1984) Dissertation, Duke University, Durham, NC.
Zanotti, G., Monaco, H. L., & Foote, J. (1984) *J. Am. Chem. Soc. 106*, 7900-7904.

On the Mechanism of Sulfite Activation of Chloroplast Thylakoid ATPase and the Relation of ADP Tightly Bound at a Catalytic Site to the Binding Change Mechanism†

Ziyun Du and Paul D. Boyer*
Molecular Biology Institute and Department of Chemistry and Biochemistry, University of California, Los Angeles, Los Angeles, California 90024-1570

Received May 8, 1989; Revised Manuscript Received July 17, 1989

ABSTRACT: Washed chloroplast thylakoid membranes upon exposure to [^{3}H]ADP retain a tightly bound [^{3}H]ADP on a catalytic site of the ATP synthase. The presence of sufficient endogenous or added Mg^{2+} results in an enzyme with essentially no ATPase activity. Sulfite activates the ATPase, and many molecules of ATP per synthase can be hydrolyzed before most of the bound [^{3}H]ADP is released, a result interpreted as indicating that the ADP is not bound at a site participating in catalysis by the sulfite-activated enzyme [Larson, E. M., Umbach, A., & Jagendorf, A. T. (1989) *Biochim. Biophys. Acta 973*, 75-85]. We present evidence that this is not the case. The Mg^{2+}- and ADP-inhibited enzyme when exposed to MgATP and 20-100 mM sulfite shows a lag of about 1 min at 22 °C and of about 15 s at 37 °C before reaching the same steady-state rate as attained with light-activated ATPase that has not been inhibited by Mg^{2+} and ADP. The lag is not eliminated if the enzyme is exposed to sulfite prior to MgATP addition, indicating that ATPase turnover is necessary for the activation. The release of most of the bound [^{3}H]ADP parallels the onset of ATPase activity, although some [^{3}H]ADP is not released even with prolonged catalytic turnover and may be on poorly active or inactive enzyme or at noncatalytic sites. The results are consistent with most of the tightly bound [^{3}H]ADP being at a catalytic site and being replaced as this Mg^{2+}- and ADP-inhibited site regains equivalent participation with other catalytic sites on the activated enzyme. The sulfite activation can be explained by sulfite combination at a P_i binding site of the enzyme-ADP-Mg^{2+} complex to give a form more readily activated by ATP binding at an alternative site.

The chloroplast, mitochondrial, and bacterial ATP synthases and the corresponding F_1 ATPases, as isolated or after exposure to ATP or ADP, retain bound ADP after removal of medium nucleotides by gel filtration. The ADP present on the enzyme has been conventionally designated as tightly bound ADP. Labeling studies with 2-azidoadenine nucleotides [see Lunardi et al. (1987), Wise et al. (1987), and Guerrero et al. (1988)] have shown that there are two types of nucleotide binding sites, catalytic and noncatalytic, and that tightly bound ADP can be present on both types of sites. Although the chloroplast F_1 ATPase (CF_1), like other F_1 ATPases, likely has three noncatalytic and three catalytic nucleotide binding sites, uncertainty remains as to whether all three catalytic sites function in an equivalent manner or whether one or more has a type of regulatory function.

One catalytic site on CF_1, like other F_1 ATPases, has a much higher affinity for ATP or ADP than the other two catalytic sites. CF_1 can be obtained with about one tightly bound [^{3}H]ADP present either by its exposure to medium [^{3}H]ADP present either by its exposure to medium [^{3}H]ADP for 1-3 h (Bruist & Hammes, 1981) or by the cleavage of [^{3}H]ATP and the removal of medium nucleotides (Wu & Boyer, 1986). Similarly, about one tightly bound [^{3}H]ADP per synthase on chloroplast thylakoid membranes can be obtained by short exposure to light and medium [^{3}H]ADP or [^{3}H]ATP [see Shavit and Strotmann (1980), McCarty and Nalin (1986), Du and Boyer (1989)]. Observations of Smith and Boyer (1976) showed that such tightly bound ADP on chloroplast thylakoid membranes was released during the initial turnover of the synthase induced by an acid-base transition. This was interpreted as resulting from the participation of the tight ADP binding site as an alternating site in the binding change mechanism. A catalytic site location for the tightly bound ADP was also indicated by the demonstration that such ADP on CF_1 (Feldman & Sigman, 1982), on thylakoid membranes (Feldman & Sigman, 1983), or on the mitochondrial enzyme (Sakamoto & Tonomura, 1983) formed bound ATP upon exposure to high concentrations of medium P_i. A catalytic site location also has been supported by several other studies (Carmeli et al., 1981; Feldman & Boyer, 1985; Drobinskaya et al., 1985) and demonstrated by labeling studies with 2-azido-ADP and 2-azido-ATP (Xue et al., 1987).

Other studies have raised the possibility that catalysis might involve other sites on the enzyme and not include the site where the readily replaceable ADP discussed above is bound. For example, in a series of studies from Hammes' laboratory the ADP was regarded as being at noncatalytic sites [e.g., see

† Supported by U.S. Department of Energy Grant P.A. DE-ASO3-7ER7102 and U.S. Public Health Service Grant GM-11094.

0006-2960/90/0429-402$02.50/0